A low density ocean inside Titan inferred from Cassini data

Sander Goossens[1*], Bob van Noort[2,3,4], Alfonso Mateo[4], Erwan Mazarico[1], Wouter van der Wal[4]

[1*]NASA Goddard Space Flight Center, MD, USA.
[2]Southeastern Universities Research Association, Washington DC, USA.
[3]Center for Research and Exploration in Space Science and Technology (CRESST) II, USA.
[4]Delft University of Technology, Faculty of Aerospace Engineering, The Netherlands.

*Corresponding author(s). E-mail(s): sander.j.goossens@nasa.gov;

Abstract

The Cassini mission has provided measurements of the gravity of several moons of Saturn, as well as an estimate of the tidal response, expressed as the degree 2 Love number $\boldsymbol{k_2}$, of its largest moon, Titan. The first estimates of Titan's Love number were larger than pre-Cassini expectations. Interior modeling suggested it may be explained with a dense ocean, but interpretation remained unclear. We have analyzed Cassini tracking data to determine Titan's gravity field and its Love number. Our gravity results are consistent with earlier studies, but we find a lower Love number for Titan of $\boldsymbol{k_2 = 0.375 \pm 0.06}$. This lower value follows from an elaborate investigation of the tidal effects. We show that a dense ocean is not implied by the obtained Love number; instead, a water or ammonia ocean is more likely. A lower density ocean can increase the likeliness of contact between the silicate core and ocean, which can leach minerals into the ocean and could promote its habitability.

The Cassini mission explored Saturn and its icy moons for more than a decade. Among its many instruments, Cassini carried a Radio Science Subsystem that enabled Earth-based radiometric tracking of the spacecraft by the Deep Space Network (DSN). These data were used to determine the gravity field and interior structure of several

of Saturn's moons [1–4], as well as that of Saturn itself [5]. Cassini data were also used to determine Titan's tidal response [6], expressed as its degree 2 potential Love number k_2. This dimensionless parameter describes how the gravitational field of a self-gravitating body is changed in response to forcing by the gravitational field of a disturbing body, which in this case is Saturn.

To explain the presence of methane on the surface of Titan, thermal modeling of its interior predicted that it could contain an internal ocean [7]. Additional modeling suggested that an ammonia-rich liquid layer may be present under an icy shell [8–10] and that Cassini might be able to detect such a subsurface ocean from measurements of Titan's Love number [11, 12]. Knowledge of the composition of the ocean, as expressed for example in its density, is important as it influences melting curves and interior temperature profiles. This in turn influences the interior layering and possible contact between ocean and silicate core, which has implications for habitability [10, 13, 14].

Initially, Titan's gravity field, without k_2, was estimated up to spherical harmonic degree and order 3 from four flybys [1]. Adding two more flybys allowed for the estimation of k_2, resulting in values of $k_2 = 0.589 \pm 0.15$ and $k_2 = 0.637 \pm 0.224$ using two different processing strategies [6]. These values confirmed the presence of a global ocean. Yet, while a dense ocean could account for the estimated k_2 range (which was larger than expected [10]), the water or ammonia-based ocean with a thin shell (generally considered to be less than 100 km), favored by evolution models, is only consistent with the lower end of this k_2 range [6].

Subsequent analyses using refined interior modeling, some with additional data from for example Titan's obliquity [15] or shape [16], found that only models with a dense ocean could satisfy the k_2 constraint [17–19]. Models of Titan's interior consistent with the moon's mean density, polar moment of inertia factor, and obliquity, were also only consistent with the lower end of the k_2 estimate; it was argued that the higher k_2 value could be matched by a denser ocean or mushy lower ice layers, but their existence was not supported by evidence [13].

Analysis of the entire set of 10 Titan flybys resulted in a Love number $k_2 = 0.616 \pm 0.067$ [3], close to the earlier results. Interpretation of the Love number remained unclear: the high value could indicate a high density ocean, a partially viscous response of the deeper regions of the moon, or a dynamic contribution to the tidal response, such as non-resonant dynamic tides [3]. An accurate determination of the Love number is thus crucial to determine the existence of an ocean and to be able to place constraints on its composition.

Results

We have processed Cassini radiometric tracking data with different tools and analysis methods from earlier efforts (see Methods, Data Analysis section). We determined gravity field models for Enceladus and Titan, including Titan's Love number. Our solutions for both moons are listed in Supplementary Table 1. We discuss results for Enceladus here for validation of our processing.

Enceladus' gravity

Following earlier work [20], we determined a degree and order 2 field for Enceladus, together with the zonal term J_3. The terms that are well-determined (i.e., with relatively small uncertainties) are J_2 and $C_{2,2}$. The zonal term J_3 has a formal error slightly larger than half of the coefficient value. The values of $C_{2,1}$, $S_{2,1}$, and $S_{2,2}$ are relatively large. These coefficients are related to Enceladus' orientation as they would be zero in a principal axis system. With only three flybys our solutions are not sensitive to these. When we constrain them to be small, the other coefficients are not significantly affected.

We find a ratio of $J_2/C_{2,2} = 3.30 \pm 0.27$ (errors are one-sigma unless indicated otherwise), which is very close to the hydrostatic equilibrium expectation of 10/3. We use the Darwin-Radau relationship [21] to determine Enceladus' polar moment of inertia factor $C/(MR^2)$ where C is the polar moment of inertia, M the mass and R the radius (252 km). We find a value of $C/(MR^2) = 0.345 \pm 0.01$ which suggests differentiation of the moon with a rocky core at its center.

Titan's gravity and tides

For Titan we estimated a full degree and order 5 field and its Love number, similar to earlier work [3]. We show Titan's radial accelerations in Figure 1. Several of the larger anomalies are below ground tracks, yet the stronger negative gravity anomaly between 60°E – 120°E and 30°N – 90°N is not and it is thus much more uncertain, as confirmed by the map of anomaly errors (Supplementary Figure 3).

We show the power in the gravity field in Figure 2, together with the power per degree of the formal errors. The power in our solution increases for degree 4 and 5, compared to degrees 2 and 3. This may be due to gaps in the geographical coverage with the flybys (see Figure 1), resulting in not enough resolution to estimate a full degree and order 5 field. This could indicate the need for constraints, but we decided not to apply constraints on the gravity coefficients (see Methods, Data Analysis section). The degree 2 and order 1 coefficients are small due to better coverage, which indicates a better sensitivity than we found for Enceladus, and agreement with the rotational model we used for Titan in our analysis [22].

Similar to Enceladus, the J_2 and $C_{2,2}$ coefficients are the coefficients that are determined best. We note that the relative errors for these coefficients are smaller for Enceladus than for Titan, despite having many fewer flybys, likely due to the larger values of the coefficients. For Titan, we find a ratio of $J_2/C_{2,2} = 3.21 \pm 0.72$. This is slightly lower than the hydrostatic ratio but within one sigma. Using the Darwin-Radau relationship we find a polar moment of inertia ratio of $C/(MR^2) = 0.348 \pm 0.03$ (where we used a radius of 2575 km for Titan). This also indicates that Titan is differentiated. Such a moment of inertia factor can also be consistent with a fully differentiated interior consisting of an icy shell over a low-density core [23].

Because the $J_2/C_{2,2}$ ratio differs from the hydrostatic value, and considering its large uncertainty, non-hydrostatic contributions may be present which would affect the inertia factor estimate [24]. This may also have an effect on librations [25]. Following earlier analysis [3], we can account for this to some extent by assuming a hydrostatic

and non-hydrostatic part for each coefficient. We then find the hydrostatic part of the total coefficient by minimizing the root-mean-square of the differences between total and hydrostatic coefficient for both J_2 and $C_{2,2}$, where the hydrostatic parts have direct expressions dependent on the fluid Love number [26], which is the Love number that characterizes the long-term rotational and tidal distortions, in the limit that the exciting period goes to infinity. This results in a slightly higher moment of inertia factor of $C/(MR^2) = 0.354 \pm 0.01$ when using the hydrostatic parts of the coefficients.

The tides raised on Titan by Saturn change Titan's degree 2 gravity field, and this effect, modeled with the Love number k_2, can be estimated directly using the response to a tidal potential or through time-variations in the degree 2 coefficients; both methods are identical (see also Discussion, and Methods, Tidal Effects section for more details). Flybys of Titan dedicated to gravity occurred at different mean anomalies of Titan in its orbit around Saturn (see the flyby characteristics in Supplementary Table 4), which increases the observability of the tides [3]. We iterated gravity solutions, gradually expanding the maximum spherical harmonic degree (see Methods, Data Analysis section). We estimated k_2 for different expansions, and base our final result on a series of degree and order 5 fields. We find a mean and standard deviation of all these solutions of $k_2 = 0.375 \pm 0.06$, and extreme values of 0.25 and 0.49. The higher values were found with low expansion degrees and when weighting the data uniformly (see Methods, Data Analysis section), but the solutions for k_2 are generally in the $0.3 - 0.4$ range. Each separate solution has a formal error close to 0.13; as indicated, our quoted error is from the spread in solutions which comes out to be half the formal error of the individual solutions.

Discussion

Flybys have only a limited sensitivity to the gravity field coefficients, due to their limited spatial coverage (see also Figures 1 and Supplementary Figure 3, and Supplementary Figure 4 for Enceladus), but at least the J_2 and $C_{2,2}$ terms should be well determined for both moons: these terms are by far the largest (due to rotational and tidal forces), and the ground track coverage for the moons is such that both terms should be determined well (there are high- and low-inclination tracks). For both Enceladus and Titan we find good agreement with earlier analyses [1, 3, 20] for these coefficients. For Enceladus our J_2 is slightly smaller and $C_{2,2}$ is slightly higher, resulting in a smaller $J_2/C_{2,2}$ ratio, but the ratio is consistent within one sigma. Our J_3 term is larger (in an absolute sense), but it also has a relatively large error. For Titan, our $J_2/C_{2,2}$ ratio is very close to that from earlier analyses [1, 3], while our individual coefficients are slightly different (see Supplementary Table 1 for a comparison with earlier results). They are generally consistent within one sigma, and thus not significantly different. These results, together with good levels of fit to the data (where close approach signals in the tracking data residuals disappear; see Methods, Data Analysis section) indicate the validity of our processing and provide confidence in our solutions.

Our reported errors are higher than those from earlier results using the same data. This may be partly due to the fact that we use 10 s data instead of 60 s data: shorter count intervals in general increase the intrinsic noise although thermal noise is deemed

minor for Cassini [27]. We also use a different data weighting scheme, and we apply variance component estimation in our estimation, where each flyby is a statistical set for which a weight factor is determined (see Methods, Data Analysis section). The formal errors from our solutions are thus calibrated such that the formal statistics match the observed statistics (i.e., variations of data residuals from cyclically randomizing the statistical sets), resulting in higher formal errors for the gravity coefficients (see also Figure 2). The error for degree 2 is larger when we estimate k_2. This is due to correlations between k_2 and the degree 2 gravity terms (see Methods, Tidal Effects section).

As stated earlier, the power in the degree 4 and 5 terms of Titan's field is larger than that of earlier analysis [3], which found the spectrum to follow a power law (Kaula rule) of $10^{-5}/n^2$ (with n the spherical harmonic degree). The higher degree expansions did not significantly affect the lower degree coefficients; our k_2 estimate was only slightly affected. We noticed that the fit to the data did not improve much when we estimated a degree and order 4 or 5 field compared to a degree and order 3 field (see Supplementary Figure 5), and this indicates that the solutions are likely not sensitive to a full 5 by 5 field. We estimate the full degree and order 5 field nonetheless to prevent possible aliasing of additional signal into the lower degree terms. We did not constrain the gravity parameters to follow a Kaula rule as the knowledge of icy bodies' gravity field is currently too limited to make definite statements about the expected power spectrum [28]. The higher degree terms are not determined well; for several, the formal error is larger than the coefficient value, which was also noted in earlier work [3].

Having established that the solutions agree for the important degree 2 terms, we next investigated differences with the earlier studies for the estimation of k_2. As indicated, our analysis can account for the effects of the tides in two separate ways: through a direct tidal potential, or through the time-varying effects on degree 2 coefficients (see Methods, Tidal Effects section). We used both tidal models separately in our processing and this results in the same estimated k_2 value.

Earlier work [6] used the approach of the time-varying effects on the degree 2 terms. We note however that there are three core differences with how the tides are accounted for, compared to our analysis. First, an approximated tidal potential [11, 12] was used, whereas we use a more general expression that does not rely on assumptions for Titan's orbit [29, 30]. Second, we note a discrepancy of a factor of 2 in the time-dependent k_2 contribution to the $S_{2,2}$ term, making the term smaller compared to the cited pre-Cassini work [11, 12] their expressions are based on. Third, the time-varying effects of k_2 on the degree 2 terms are not correctly accounted for in the partial derivatives; these relate changes in the data residuals to changes in the k_2 parameter and are critical to form linearized observation equations and estimate the parameter.

Because the effects of k_2 on the degree 2 terms are time-dependent, they should be accounted for by combining them with the partials for the degree 2 gravity terms in the numerical integration of the variational equations. However, in the earlier analysis of Cassini data [6] they are combined with the degree 2 terms after the variational equations are integrated. We show that this results in an observation equation system

that does not correctly relate changes in the estimated parameters with changes in the data residuals (see Methods, Estimation of k_2 section).

When we alter our own estimation scheme to follow the earlier analysis, we can replicate their results: we then also obtain larger Love numbers (see Supplementary Table 2). The first difference is likely of little consequence as the approximated tidal potential is close to the more general one (see Methods, Tidal Effects section). The discrepancy in the $S_{2,2}$ factor by itself also should in principle not influence the results too much, because the J_2 and $C_{2,2}$ effects of k_2 are much larger (see the discussion of the permanent contributions to the degree 2 terms in the Methods, Tidal Effects section). But constructing the partials from which k_2 is estimated without taking into account the effect of k_2 on the degree 2 terms during the numerical integration of the variational equations compounds with the other two differences, and results in an over-estimation of k_2.

We can reproduce the earlier results with the incorrect partials. A later solution [3] may have used the correct partials (priv. comm.), yet this is not documented. They find results very consistent with the earlier ones ($k_2 = 0.616$), which is surprising as we find a strong influence of the partials on the resulting value, and we thus would expect at least a change in the k_2 value when using different tidal modeling. We cannot reproduce the later results with using the correct partials. We also cannot explain the differences in k_2 with the use of constraints or by using a different maximum degree and order of the expansion. When we use the later results [3] as a starting point in our analysis, including k_2, we still find a lower Love number. Our results never reach high k_2 values; we therefore conclude that the application of the correct partials leads to a Love number estimate that is robustly in the range of 0.3 to 0.4.

Analyses of interior models for Titan based on the higher Love number found a need for a dense ocean to match the Love number constraint, which often was still only satisfied at the lower end of its uncertainty. Our lower value is closer to pre-Cassini predictions [10]. Together with our estimate for Titan's moment of inertia, and its bulk density (obtained from the value of GM, see Supplementary Table 1), we can use the Love number to determine parameters of an interior structure model of Titan to probe whether a dense ocean is still implied. For completeness we also include Enceladus in our analysis but we discuss results only in the Methods, Interior Modeling section.

We model Titan's interior as a spherically symmetric body. We assume 4 layers: a rocky core, a high-pressure ice shell, an ocean, and an icy crust [14, 17, 31], with a fixed total radius of 2575 km. We computed realistic density profiles for the hydrosphere based on recent analysis [31] for varying ocean compositions (pure water, and varying weight percentages of $MgSO_4$) and temperatures at the bottom of the ice shell (which is a proxy for the shell thickness), and compared the tidal response of such profiles to that of a model with layers of constant density (where the constant density was the average of the density profile in each layer; all other parameters, which are discussed below, were kept the same). We show such a density profile in Supplementary Figure 11. We found that accounting for the increase of density with depth increases the Love number by at most 4 %, which is smaller than the current error on k_2, and in agreement with earlier results [17].

Given the large impact of the ocean density on the predicted Love number [14, 17, 31] and the significantly lower Love number, we find it more prudent to use a simplified model with parameters that previous analyses have shown to have the most influence on k_2. We thus use a model with constant densities in our subsequent analysis.

We vary the core radius and density, ocean thickness and density (the ice shell thickness also varies; it is determined automatically from the fixed planet radius and other radii values), the viscosity of the high-pressure ice and icy crust, within given limits (see Methods, Interior Modeling section, and Supplementary Table 3 for values and their ranges). We explore the parameter space using a Markov Chain Monte Carlo (MCMC) approach [32] to match the moment of inertia factor (we use our value of $C/(MR^2) = 0.348 \pm 0.03$), bulk density, and Love number. To compute Titan's tidal response we used a Maxwell rheology for Titan but find that we obtain the same results with an Andrade rheology.

We find that the moment of inertia factor is mostly sensitive to the core parameters. The error on the polar moment of inertia factor is such that we cannot determine the ocean thickness or icy crust thickness with certainty. We generally find solutions close to our minimum ocean thickness (50 km) but thicker oceans are also possible. We show histograms for the core radius and density in Figure 3, and the distribution for all parameters and measurements in Supplementary Figure 12 which allows for additional considerations of the sensitivity of our results. We find a core size of 2110 ± 76 km and a core density of 2528 ± 175 kg/m^3 from the modes of the distributions. Both of these values are consistent with models from a recent review of Titan's interior [14].

We show the relationship between ocean density and k_2 in Figure 4 as a heat map of model counts from our results. Our analysis clearly favors lower densities for Titan's ocean. We obtain an ocean density of 1091 ± 107 kg/m^3 as the mean and standard deviation of the distribution of ocean densities. Larger densities are less likely, and indeed result in larger Love numbers. A dense ocean is thus not implied to match our estimate of Titan's Love number.

We tested a wide range of viscosities and rigidities for the layers pertinent to the tidal response, and the results showed only low sensitivities, similar to an earlier study [17]. Our simplified modeling may result in weaker sensitivities with respect to the viscosities and rigidities than when more complete models with temperature-dependent viscosity profiles are used. Such models would include viscosity changes with depth which will affect the tidal response. Still, studies that apply more complete models all indicate that a lower Love number correlates with lower ocean densities [13, 17, 31].

Ocean density depends on its composition [31], and it also affects the thickness of the crust and high-pressure ice layer through its effect on temperature profiles [14]. A thin icy crust and a less dense ocean may result in a thin or even absent high-pressure layer. This in turn would make contact between the ocean and core more probable, and increases the chance that volatiles and organics in the core could be transported into the ocean with implications for astrobiology [14]. Previous analyses of Titan's interior using the higher Love number value focused on increasing the ocean density by looking at different compositions. An ocean with a higher weight percentage of $MgSO_4$ has a higher density compared to pure water or an ocean with NH_3[31]; our lower Love

number implies a lower density which favors water or NH_3 oceans. Our results thus have important implications for our knowledge of Titan's interior structure, ocean composition, and potential habitability.

Methods

Data Analysis

We processed DSN radiometric X-band tracking data in continuous spans of time called "arcs", using the NASA GSFC GEODYN II software [33]. We did not include data with X-band for the uplink and Ka-band for the downlink; the Sun-Earth-Probe angles [3] are such that plasma effects are likely small. We numerically integrate the equations of motion for both the central body (Enceladus or Titan) and the spacecraft, using high-fidelity models for the forces. The forces on the spacecraft include the following: the central body's gravity field (and tides, for Titan); third body perturbations by Saturn, its seven largest moons (Iapetus, Dione, Enceladus or Titan, Mimas, Tethys, Rhea, and Hyperion), and the solar system bodies (including the Moon and Pluto); Saturn's gravity (its zonal harmonics) and its rings [5]; solar radiation and drag (we include a model of Cassini's shape in our analysis); and accelerations induced by the radioisotope thermoelectric generators (RTG). For the RTG accelerations we use the model applied to Cassini by earlier analysis, taking into account the half-life of plutonium [1, 34]. For the central bodies the forces consist of the gravitational forces of the other bodies. We use rotational elements for Enceladus recommended by the International Astronomical Union [35]; for Titan we use those from Cassini results [22]. For the positions of the moons and bodies as well as the initial position and velocity of Cassini we use values from a reconstructed trajectory [36], which are based on JPL planetary ephemeris DE435 and Saturn satellite ephemeris SAT409.

We model the measurements using highly accurate and state-of-the art models, including but not limited to effects from the troposphere and ionosphere, and effects from ocean loading on the DSN sites. All flybys used the High-Gain Antenna except for T110 which used the Low-Gain Antenna (LGA). We model the positions of each. We clearly see the signal of antenna motion in T110 if we do not use updated LGA coordinates [37].

We divide the set of estimated parameters into two groups: local parameters that only affect measurements in one arc, and global parameters that affect measurements for all arcs. The local parameters are the following: the state (position and velocity) at initial epoch for both the spacecraft and central body, a scaling coefficient for solar radiation pressure, scaling coefficients in the spacecraft frame for the RTG accelerations, and a measurement bias for 3-way Doppler data (different transmitting and receiving stations) to account for differences in reference frequency at the stations. We only used 3-way data if they were collected during closest approach; they were then used in addition to 2-way data, just because this is the most important time-span of the data collection. We also estimate a drag scaling coefficient for each Titan flyby, and velocity adjustments at closest approach for two of the three Enceladus flybys to account for the effects of plumes [20]. The global parameters are the coefficients of a

spherical harmonic expansion of the gravity field, the body's gravitational parameter GM, and for Titan its Love number k_2.

For the ten flybys dedicated to Titan gravity we processed the data in arcs with an average length of slightly more than 2 days, excluding spacecraft maneuvers, thruster firings, or angular momentum desaturation events that could impart residual accelerations on the spacecraft. For Enceladus, there were three flybys dedicated to gravity. We processed these data in arcs with lengths slightly over one day. For each arc, we process the data to adjust the local parameters. We compare the modeled measurements with the actual observations (their differences are the residuals) and adjust the local parameters in a batch least-squares sense [38, 39]. The arc is considered converged when changes in the root-mean-square of the residuals are 1% or less. We then generate partial derivatives of the measurements with respect to all parameters and form the normal equation system. The normal equations from all flybys for one body are then combined, where weights per flyby are determined using variance component estimation [40] (VCE; see below). We repeat this entire process (estimation of local and global parameters) several times until the results are deemed to have converged (see below).

We use 10-second averaged data for the flybys of both bodies. We weighted the data uniformly at 28 mHz during determination of the local parameters, corresponding to 0.5 mm/s for X-band data. Because we use 10 s data our root-mean-square values for the fits are generally a little higher than those for earlier analysis [3], where 60 s data were used. We show an example of data residuals before and after gravity estimation in Supplementary Figure 1. The closest-approach signal is clearly visible in the residuals before gravity estimation. After gravity adjustment, the residuals resemble data noise. If we use 60 s data, the fit improves at a level commensurate with the longer count interval, as expected. We have no indication that the higher intrinsic noise level of 10 s data affects our results; as mentioned in the main text, thermal noise is deemed to be minor for Cassini [27]. We selected the shorter count interval to ensure a good sampling of the gravity field. At Titan (with flyby speeds around 6 km/s with respect to the moon) this is not an issue due to its large size, but at Enceladus (at flyby speeds between 6.5 and 7.5 km/s) a degree 2 field may run the risk of being undersampled when using 60 s data. We show the root-mean-square of data fit in Supplementary Figure 2. We clearly fit well below the data weight of 28 mHz. If we use the gravity model from earlier Cassini analysis [3] for our Titan analysis, we obtain similar fits as with our own model.

We apply constraints during the determination of the local and global parameters, but mostly they are weak. Generally the parameters adjust at levels well below their constraint. We leave Cassini's state (position and velocity) unconstrained. The central body's state during the determination of the local parameters is constrained (at 1 mm and 0.01 mm/s) as we found this generally resulted in better data fits, but we apply weak constraints when we solve the combined normal equation systems because the states affect the other parameters: for Enceladus we used 500 m for positions, 10 m/s for velocities, and for Titan we used 5 km for positions and 100 m/s for velocities. The results for Enceladus did not change significantly if we used the constraints also used for Titan's state. We apply a constraint of 10% to solar radiation pressure coefficients,

6% to drag coefficients (for Titan; for most flybys drag is not needed and for low-altitude flybys the drag coefficients have small adjustments on the order of 0.3×10^{-4} from their nominal value of 2.4), 1 mm/s for velocity adjustments (Enceladus), 0.001 for the RTG accelerations in xyz directions in the spacecraft frame (for a nominal value of 1; on average they adjust at 2 or 3 orders of magnitude below the constraint), and 1 mHz for Doppler 3-way biases. All of these parameters have only very small adjustments, and they do not influence the gravity solutions. All other parameters, such as the gravity field, GM, and Love number, are unconstrained.

As stated above, we repeat this process many times, starting with knowledge of only the GM of the flyby body (8978 km^3/s^2 for Titan and 7.21044 km^3/s^2 for Enceladus; all other gravity terms are set to zero), initially estimating only a degree and order 2 field, and gradually increasing the number of spherical harmonic coefficients (in the case of Titan; for Enceladus we included only J_3 after several iterations). We consider these global iterations converged when the residuals fit close to noise level (a few mHz) and do not change significantly between iterations ($< 1\%$). Data fit did not change much with each increase in expansion (see also Supplementary Figure 5), so regardless of changes in fit, we decided to run 10 global iterations for each model expansion. Convergence generally was reached well before that. Supplementary Figure 5 indicates that for several flybys the fit hardly improved. We noticed that in those cases local parameters (most notably, Cassini's initial state) showed large adjustments for the case with no gravity field knowledge (only GM), and much smaller adjustments after determination of the gravity field.

When using VCE in our gravity determination, each flyby is a separate statistical set. VCE determines scale factors on each set with the goal to balance the formal error statistics with observed statistics (i.e., variations of residuals from cyclically randomizing the statistical sets [40]), and it calibrates the covariance. We show the VCE factors and resulting effective data weights in Supplementary Table 4. Factors larger than one mean that the data are up-weighted. Because we fit better than our initial data weight for all flybys, all flybys are up-weighted, some more than others. Note that we did not change the data weights in the determination of the local parameters, but always used 28 mHz. We use only one data type (Doppler), and because of this the data weight does not affect the values of the local parameters (the weights then only affect the formal errors of the local parameters for each arc, before combining them into one larger system).

We determined k_2 during various expansions of the gravity field model to test the stability of the parameter estimation. We base our final result on the values obtained with a series of degree and order 5 fields. We determine our k_2 value as the uniformly weighted average of estimated k_2 values from these global iterations, and the presented uncertainty is the standard deviation of these values around the mean. The set of k_2 values from the degree and order 5 fields were either estimated with the data weighted uniformly at 28 mHz, or the data weighted with the aforementioned VCE factors. We note that in general the results from uniformly weighted data produce slightly higher k_2 values than those with the VCE factors.

We show Enceladus' gravity and its associated errors expressed as radial accelerations in Supplementary Figure 4, including the ground tracks for the flybys. The

anomalies that are visible are related to ground track coverage; their location is largely determined by the resulting $C_{2,1}$, $S_{2,1}$, and $S_{2,2}$ coefficients. The sign for J_3 results in a negative anomaly over the south pole of Enceladus. similar to earlier work [20].

Modeling of the tidal effects

The tidal potential U_t can be expressed as [21]

$$U_t = \frac{GM_s}{r_s^3} r^2 P_{2,0}(\cos\psi), \tag{1}$$

where GM_s is Saturn's GM (the disturbing body), r_s is the distance to Saturn, r the distance to the computation point, ψ is the angle between the computation point and the center of Saturn, and $P_{2,0}(\cos\psi)$ is the unnormalized degree 2 Legendre function,

$$P_{2,0}(\cos\psi) = \frac{1}{2}\left(3\cos^2\psi - 1\right). \tag{2}$$

A general expression for the tidal potential can be obtained by using the addition theorem for Legendre functions,

$$P_{n,0}(\cos\psi) = \frac{1}{2n+1} \sum_{m=-n}^{m=n} \bar{Y}_{n,m}(\phi',\lambda')\, \bar{Y}_{n,m}(\phi,\lambda), \tag{3}$$

where n and m are the degree and order, respectively, (ϕ',λ') and (ϕ,λ) are coordinate pairs and ψ is the angle between them. The function $\bar{Y}_{n,m}(\phi,\lambda)$ is defined as

$$\bar{Y}_{n,m}(\phi,\lambda) = \bar{P}_{n,|m|}(\sin\phi) \begin{cases} \cos m\lambda, & m \geq 0 \\ \sin|m|\lambda, & m < 0 \end{cases}. \tag{4}$$

The planet's response is equal to the Love number times the tidal potential. Application of the addition theorem in equation (1) (generalizing to all degrees n instead of limiting to degree 2) results in expressions for time-varying changes $\Delta\bar{C}_{n,m}$ and $\Delta\bar{S}_{n,m}$,

$$\Delta\bar{C}_{n,m} - i\Delta\bar{S}_{n,m} = \frac{k_{n,m}}{2n+1}\frac{GM_s}{GM_t}\left(\frac{R_t}{r_s}\right)^{n+1} \bar{P}_{n,m}(\sin\Phi_s) e^{-im\lambda_s}, \tag{5}$$

where GM_t is Titan's GM, R_t its radius (2575 km), $\Delta\bar{C}_{n,m}$ and $\Delta\bar{S}_{n,m}$ are changes to the normalized gravity field coefficients, (λ_s,Φ_s) are the coordinates of Saturn with respect to Titan in Titan's body-fixed frame, and $k_{n,m}$ are Love numbers, now per degree and order. The ratio of radii relates to the attenuation with distance. These coordinates, together with r_s which describes the distance between Saturn and Titan, vary with time and hence this results in time-varying coefficients. This is the general expression as used by the International Earth Rotation and Reference Systems

Service [29, 30] (IERS). For spherically symmetric planets, there is no dependency on order, and the Love number per degree is simply k_n.

Instead of using changes in the degree 2 gravity coefficients (limiting ourselves now to only degree 2), a direct expression of the tidal potential can also be used,

$$U_t = \frac{k_2}{2}\frac{GM_s}{r_s^3}\frac{R_t^5}{r^3}\left(3(\hat{\mathbf{r}}_s \cdot \hat{\mathbf{r}})^2 - 1\right), \tag{6}$$

where $\hat{\mathbf{r}}_s$ is the unit vector between the centers of Titan and Saturn, and $\hat{\mathbf{r}}$ is the unit vector from Titan's center to the position where the potential is calculated. This expression can be obtained from eq. (1) through the definition of the in-product and the angle between 2 vectors. Both expressions are equivalent, and both implementations are possible with our analysis software. We obtain the same k_2 from them.

The tidal potential can be expressed differently when certain assumptions about Titan's orbit are made. Titan's orbit has a small inclination and eccentricity. Under these assumptions, the potential can be expressed in terms of Titan's eccentricity e and mean anomaly M, and it follows readily that eq. (5) includes a static and periodic part [12]. This results in expressions for changes in the degree 2 coefficients $C_{2,0}$, $C_{2,2}$, and $S_{2,2}$,

$$\Delta C_{2,0} = \Delta C_{2,0}^{\text{static}} + \frac{1}{2}k_2\, q_t\, e\cos M, \tag{7}$$

$$\Delta C_{2,2} = \Delta C_{2,2}^{\text{static}} - \frac{1}{4}k_2\, q_t\, e\cos M, \tag{8}$$

$$\Delta S_{2,2} = \Delta S_{2,2}^{\text{static}} - \frac{1}{3}k_2\, q_t\, e\sin M, \tag{9}$$

where q_t is defined as

$$q_t = -3\frac{GM_s}{GM_t}\left(\frac{R_t}{a}\right)^3. \tag{10}$$

with a the (constant) semi-major axis of Titan's orbit. In this case the coefficients are unnormalized. Such expressions are convenient because they allow for the separation of the static and periodic effects: one can estimate k_2 from only the periodic contributions to the degree 2 terms, and this is how it was done in previous analyses [3, 6]. It should then also be made clear that the contribution of the permanent tide is accounted for in the static gravity field coefficients (J_2, $C_{2,2}$, and $S_{2,2}$). Such coefficients are called "zero tide" [30]. If the contribution of the permanent tide is not included, the degree 2 coefficients are called "conventional tide free" [30].

From eq. (5) it is not readily clear that there is a permanent tide contribution. It is only explicit for $\Delta\bar{C}_{2,0}$ because $\bar{P}_{2,0}$ has a constant term (eq. 2). But using Taylor expansions for small angles Φ_s and λ_s, it will be clear that there are also constant terms for the order 2 coefficients $\Delta\bar{C}_{2,2}$ and $\Delta\bar{S}_{2,2}$.

Separating the permanent and periodic contributions and using only the periodic terms to estimate k_2 results in lower correlations between k_2 and the degree 2 gravity terms. With the permanent contribution included the correlation between $\bar{C}_{2,0}$ and k_2 is 0.96 and that between $\bar{C}_{2,2}$ and k_2 is -0.99; they are lowered to 0.36 and 0.13 when

the permanent contribution is removed. Our analysis shows it also results in lower formal errors but without changing the estimated value itself. Without k_2 estimation, our solution also resulted in a lower error at degree 2 (see Figure 2). Our analysis mostly used eq. (6) to account for the tides. From this expression it is not readily clear that there is a constant for certain degree 2 terms; there is a constant term in the potential but it still depends on r_s which varies with time. The same assumptions about Titan's orbit could be made to isolate a constant contribution to the tidal potential of eq. (6), but we used the expression as is. Our formal error at degree 2 is thus higher (Figure 2) but this did not affect the value of the estimated coefficients.

While some assumptions are made to obtain the expressions in eqs. (7) – (9), these assumptions are very reasonable. Differences in time-variations of the degree 2 terms between the two sets of expressions (eq. 5 and eqs. 7 – 9) are small (see Supplementary Figure 6). We note that the simplified potential does not have time variations for the degree 2, order 1 terms, whereas those from eq. (5) have. They are however much smaller than those for the other terms (see Supplementary Figure 7).

Estimation of k_2

The general linearized observation equation that relates changes in data residuals $\Delta\rho$ to changes in parameters $\Delta\mathbf{p}$ is given as

$$\Delta\rho = \mathbf{A}\ \Delta\mathbf{p}, \tag{11}$$

where $\mathbf{A}$ is the partial derivative matrix that relates the two. Partial derivatives are obtained through the numerical integration of the variational equations [38, 39].

The Love number k_2 is estimated from tracking data through its effect on the gravity field of the central body. As explained above, the tides raise a potential and thus a force; this potential can be expressed directly as in eq. (6), or it can be related to time variations in the degree 2 gravity coefficients as in eq. (5).

When using the time-variable effect of k_2 on the degree 2 terms, c.f. eq. (5), the generation of the k_2 partials requires chaining the effects of degree 2 coefficients (denoted $\nu_{n,m}$ to indicate both $C_{n,m}$ and $S_{n,m}$ coefficients, where $m < 0$ denotes the $S_{n,m}$ terms and $m \geq 0$ denotes the $C_{n,m}$ terms) with partials of those coefficients with respect to k_2. Such partials $\partial\nu_{n,m}/\partial k_2$ can be obtained, either from eq. (5) for the general case, or from eqs. (7) – (9) for the approximated case.

In previous work [6] the partials of measurements with respect to k_2 are expressed through their effects on the degree 2 coefficients as follows,

$$\frac{\partial\rho}{\partial k_2} = \sum_{m=-2}^{m=2} \left[\frac{\partial\rho}{\partial\nu_{2,m}} \frac{\partial\nu_{2,m}}{\partial k_2} \right]. \tag{12}$$

The partials $\partial\rho/\partial\nu_{2,m}$ are obtained as output from the orbit determination (and thus, after numerical integration of the variational equations), and they are then multiplied afterwards with the respective k_2 partials, evaluated at the time of the observation, to obtain the total partial for k_2. However, the partials $\partial\nu_{2,m}/\partial k_2$ are time-dependent

but in this way this time-dependence is not accounted for in the integration of the variational equations.

The variational equations for estimating model parameters $\mathbf{p}$ are obtained from the equations of motion that relate the spacecraft state $\mathbf{x}$ (both position and velocity), the parameters, and forces $\mathbf{f}$ acting on the spacecraft through

$$\frac{d}{dt}\mathbf{x} = \mathbf{f}(t, \mathbf{x}, \mathbf{p}) = \dot{\mathbf{x}}(t, \mathbf{x}, \mathbf{p}). \tag{13}$$

The variational equations can then be derived as

$$\frac{d}{dt}\frac{\partial \mathbf{x}}{\partial \mathbf{p}} = \frac{\partial \dot{\mathbf{x}}}{\partial \mathbf{x}}\frac{\partial \mathbf{x}}{\partial \mathbf{p}} + \frac{\partial \dot{\mathbf{x}}}{\partial \mathbf{p}}. \tag{14}$$

For clarity, using only k_2 for $\mathbf{p}$, this would read

$$\frac{d}{dt}\frac{\partial \mathbf{x}}{\partial k_2} = \frac{\partial \dot{\mathbf{x}}}{\partial \mathbf{x}}\frac{\partial \mathbf{x}}{\partial k_2} + \frac{\partial \dot{\mathbf{x}}}{\partial k_2}. \tag{15}$$

The partial $\partial\dot{\mathbf{x}}/\partial k_2$ is obtained by chaining it with $\partial\nu_{2,m}/\partial k_2$. To illustrate, if we limit ourselves to the effect of k_2 on $\bar{C}_{2,2}$ (to avoid summation over all five degree 2 terms), this partial has to be chained in the following way:

$$\frac{\partial \dot{\mathbf{x}}}{\partial k_2} = \frac{\partial \dot{\mathbf{x}}}{\partial \bar{C}_{2,2}}\frac{\partial \bar{C}_{2,2}}{\partial k_2}. \tag{16}$$

Here, normalized coefficients are used because the coefficients in the processing software are normalized. For the variational equation this results in

$$\frac{d}{dt}\frac{\partial \mathbf{x}}{\partial k_2} = \frac{\partial \dot{\mathbf{x}}}{\partial \mathbf{x}}\frac{\partial \mathbf{x}}{\partial k_2} + \frac{\partial \dot{\mathbf{x}}}{\partial \bar{C}_{2,2}}\frac{\partial \bar{C}_{2,2}}{\partial k_2}. \tag{17}$$

The partial $\partial\bar{C}_{2,2}/\partial k_2$ varies with time and thus has to be accounted for directly during the numerical integration of the variational equations. When using eq. (12) this is not the case. Only $\partial\rho/\partial\nu_{2,m}$ is obtained through the variational equations.

This results in different partials. We show the difference between k_2 partials obtained through the variational equations and those without (i.e., following eq. 12) in Supplementary Figure 8 for flyby T022. We call the latter partials "non-variational", with the understanding that the partial $\partial\rho/\partial\nu_{n,m}$ in fact is a result obtained through the variational equations; it is just that it is then multiplied with the $\partial\nu_{n,m}/\partial k_2$ partial. For this example, we used the formulation from eq. (5) in order to make sure we have the same $\partial\nu_{n,m}/\partial k_2$ values (this thus excludes the factor of 2 error in the $S_{2,2}$ term; see discussion below). It is clear that these k_2 partials are different, especially after the closest approach. This thus has an effect on the estimation of k_2 because the partials in the matrix $\mathbf{A}$ in eq. (11) will be different.

We can test if indeed changes in k_2 predict changes in data residuals by using eq. (11). We propagate an orbit for a span of time, using a value k_2^a. We compute tracking

data residuals for this value. We then perturb k_2^a into $k_2^b = k_2^a + \Delta k_2$, and compute new residuals. We then use eq. (11) to test the partial. If all is correct, then the difference in residuals should be matched by the partial times the change in k_2.

We show residual changes and predicted changes in Supplementary Figure 9. Instead of using a Cassini flyby, we used an example from the processing of Gravity Recovery and Interior Laboratory (GRAIL) inter-satellite Ka-band range-rate data, simply because a satellite in orbit around a body is more sensitive to tidal effects. The principle as well as the result is the same however as if we were to use Cassini data: small changes in parameters should result in changes in residuals as predicted by the partials in the linear regime. We perturbed k_2 by 0.02 for a nominal value of 0.024, which is a relatively large change. Supplementary Figure 9 shows that the changes in residuals match when the partials are computed with the variational partials (showing that the linearization holds despite the relatively large change in k_2), but the differences are large when they are computed with the non-variational partials. This clearly shows that the non-variational partials do not satisfy the basic observation equation, eq. (11).

In addition, to illustrate how this affects the analysis of Cassini data, we show the difference in predicted residuals between those from the variational partials and those from the non-variational partials for flyby T022 in Supplementary Figure 10. For this case we used a Δk_2 of 0.25. This shows that the difference in partials as shown in Supplementary Figure 8 results in residual differences that increase after the closest approach. This indicates the extent to which the observation equation, eq. (11), is not satisfied with the non-variational partials.

Finally, we investigated the effect on the estimation of k_2. We only focused on a case where initially $k_2 = 0$, and we did not iterate this. We selected the case $k_2 = 0$ to avoid differences in the tidal model which would lead to differences in the orbits and partials. The results from this test will therefore be different from our final solution of k_2. Here we only want to demonstrate the influence of different partials on the estimation of k_2. We thus make sure that the base ingredients for the tests that follow hereafter are the same for each case.

We generated partial derivatives for the entire Cassini data set from our standard processing. We then use either the direct partials, or we replace them with partials computed from eq. (12). For the latter, we can either use the IERS expressions or the approximated expressions[12] to compute $\partial \nu_{2,m}/\partial k_2$. We also note that in the earlier results for Titan [6], there is a mistake in the expression for $S_{2,2}$. The periodic term for $S_{2,2}$ has a factor of 1/6 where it should be 1/3, see eq. (9) [12]. We will also test the effect of this. Related to this, we generated partials from our standard processing but without the constant contributions to the degree 2 terms (while still using the fully variational approach). With this we corrupt the $S_{2,2}$ contribution with a factor of a half to test this effect. We show results for k_2 for various cases in Supplementary Table 2.

The results indicate a large influence of the choice of partials: not using the full variational approach but with the same IERS expressions from eq. (5), listed as the case "non-variational partial; IERS", already changes the k_2 value. Results with the non-variational partials are in general higher than the result with the variational

partial. The range of the k_2 values that we obtain is however within the error bars of our own estimate. Yet when we include the mistake in the $S_{2,2}$ partial, the value for k_2 further increases and is much closer to that reported before [3, 6]. Thus, we can replicate the earlier results by using the approximated tidal potential together with the mismatch in the $S_{2,2}$ term and the non-variational partials. Leaving out the permanent contributions to the degree 2 terms does not significantly affect the k_2 value when using the variational partials. The error in the $S_{2,2}$ term does increase the k_2 value but not as much as when the non-variational partials are used. While the partial differences in Supplementary Figure 8 and the residual differences in Supplementary Figure 10 may seem small, this inversion test shows that there is a strong effect on the estimation of k_2.

The fact that the $S_{2,2}$ partial has such a big influence is somewhat surprising, as it is expected that the estimation of k_2 is mostly driven by $C_{2,0}$ and $C_{2,2}$ variations. As mentioned above, if we corrupt the $S_{2,2}$ contribution with a factor of 2 in our own processing using the fully variational partials, we do not see such a large increase in the estimated k_2 value. However, when correcting for the permanent contributions to k_2 by the degree 2 terms, the size of the time-varying $S_{2,2}$ coefficient becomes comparable to the contribution of $C_{2,0}$ and $C_{2,2}$. This means that the $S_{2,2}$ term has a larger effect than when the permanent contribution to k_2 is not separated. This explains the relatively large contribution of the $S_{2,2}$ term in the previous analysis.

The degree 2, order 1 terms which are assumed to be zero in the approximated approach [12] indeed do not contribute much to the estimation of k_2, which we tested by excluding them.

Interior Modeling

We model the interior of Enceladus and Titan using homogeneous layers. For Enceladus we assume a three layer model with a core, ocean, and crust. We acknowledge that variations in Enceladus' ice shell thickness can have an influence [41], but we are not considering Enceladus' tidal response in this work. We fix the density of the ocean and crust because we only have the moment of inertia factor to constrain the radial density profile, and the density contrast between ocean and icy crust is probably difficult to resolve from the constraints. The ocean density is set to 1020 kg/m^3 and that of the (icy) crust to 925 kg/m^3; this is in the range that we use for Titan (see below) and follows earlier work [17]. The core density is then computed to match the bulk density of 1611 kg/m^3 which is obtained from Enceladus' GM (see Supplementary Table 1) and its radius of 252 km. For a three layer model, the core density ρ_c depends then on the core radius and ocean thickness following

$$\rho_{\text{core}} = \frac{\rho_{\text{bulk}} R_e^3 - \rho_{\text{ocean}} \left(r_{\text{ocean}}^3 - r_{\text{core}}^3\right) - \rho_{\text{ice}} \left(R_e^3 - r_{\text{ocean}}^3\right)}{r_{\text{core}}^3}, \tag{18}$$

where R_e is Enceladus' radius, ρ_{bulk} the bulk density, and the other densities and radii refer to the other layers.

We use a Markov Chain Monte Carlo analysis, using the open source "emcee" software [32], to explore Enceladus' structure by varying core radius and ocean thickness to match the bulk density (with a 2% error) and polar moment of inertia factor ($C/(MR^2) = 0.345 \pm 0.01$). We assume an ocean thickness of at least 5 km and also ensure that the icy crust is at least 10 km thick. We can include more parameters to vary but this does not change the fact that the solutions are mostly only sensitive to core radius and density. We ran 100,000 models using 40 chains. We find we can only resolve the core parameters. We show histograms for the core radius and core density in Supplementary Figure 13. We find a core radius of 201 ± 12 km and a density of 2202 ± 242 kg/m^3 from the modes of the distributions. This is a slightly larger core with a lower density than earlier analysis [42] but still consistent considering the errors that we obtain.

We model Titan's structure in much the same way with 4 layers: a core, high-pressure ice, ocean, and a crust. We vary core radius and density, ocean thickness and density, the viscosity of the high-pressure ice and crust, and the core's unrelaxed rigidity. Because we include Titan's k_2 as a measurement, we have to include rigidities, viscosities, and bulk moduli as well. We use values from earlier work [17] for the fixed parameters. We fix the density of the high-pressure ice to 1340 kg/m^3 and that of the icy crust to 925 kg/m^3 following earlier work [14, 17]. We also set the thickness of the high-pressure ice to 150 km, following earlier work [14] and considering lack of sensitivity. Our results do not change significantly if we vary the thickness of this layer. To compute Titan's Love number, we fix the bulk moduli for all layers: 200 GPa for the core, 20 GPa for the high-pressure ice, 2.5 GPa for the ocean, and 10 GPa for the icy crust [17]. We fix unrelaxed rigidities (shear moduli) for all but the core: 10 GPa for the high-pressure ice, 0 for the ocean, and 3 GPa for the icy crust [17]. A recent analysis [31] found different shear and bulk moduli for the core than an earlier analysis [17]. We find that changing these parameters has only a very small effect on k_2, which was also found by the earlier analysis. We used a Maxwell rheology for Titan but find that we obtain the same results with an Andrade rheology.

We list the values, and ranges for those parameters that are varied in Supplementary Table 3. For Titan we assume an ocean thickness of at least 50 km, and an icy crust thickness of also at least 50 km. Density inversions are not allowed, thus the ocean density will always be between 925 and 1340 kg/m^3 (we do not limit it to be at least 1000 kg/m^3 but this does not affect the results). For this Markov Chain Monte Carlo analysis we compute 500,000 models with 40 chains to match the bulk density (with again a 2% error), the moment of inertia ($C/(MR^2) = 0.348 \pm 0.03$), and the Love number ($k_2 = 0.375 \pm 0.06$).

We model Titan's tidal response using the open source software TidalPy [43]. We use a Maxwell rheology. When we use an Andrade rheology, we use parameter values $\alpha = 0.3$ and $\zeta = 1.0$. We did not explore variations of these parameters.

Data availability

Cassini radio tracking data and ancillary information can be found at the Planetary Data System's Atmospheres node (https://pds-atmospheres.nmsu.edu/

data_and_services/atmospheres_data/Cassini/inst-rss.html). Results from our analysis such as the gravity field models and output from our MCMC modeling can be found at https://pgda.gsfc.nasa.gov/products/91 or through https://doi.org/10.60903/gsfcpgda-titank2.

Code availability

We used the TidalPy [43] open source software for the analysis of Titan's Love number (https://zenodo.org/record/7017560), and the "emcee" open source software [32] for our Markov Chain Monte Carlo analysis (https://emcee.readthedocs.io/en/stable/). We also used the PlanetProfile software [44] (https://github.com/vancesteven/PlanetProfile) to compute self-consistent interior models for Titan used in our modeling. The input data for the MCMC analysis are the results presented in this work; additional input parameters for TidalPy are discussed in the text and listed in Supplementary Table 3. We also used the Python package "corner" [45] for the distribution plot in the Supporting Materials. We cannot provide the software used for the analysis of Cassini tracking data, but the methods have long been established and are described in detail in the methods section. All figures (apart from the distribution plot, Supplementary Figure 12) were drawn with the free GMT software [46] (https://www.generic-mapping-tools.org/).

Acknowledgments

This work was funded by NASA's Cassini Data Analysis Program (SG, BvN, EM). We thank Terence Sabaka (NASA/GSFC), Stefano Bertone (NASA/GSFC, UMBC, CRESST II), Wade Henning and Joe Renaud (NASA/GSFC, UMD, CRESST II), Gael Cascioli (NASA/GSFC, UMBC), and Daniele Durante and Luciano Iess (Sapienza University of Rome, Italy) for discussions.

Corresponding author

Correspondence and requests for materials to Sander Goossens (sander.j.goossens@nasa.gov).

Contributions

SG and EM conceived and designed the study. SG, BvN, and AMA analyzed Cassini tracking data. EM supported Cassini tracking data analysis. WvdW provided theoretical support. All authors contributed to the discussion and interpretation of the results. SG wrote the first draft of the paper. All authors contributed to subsequent drafts.

Competing interests

The authors declare no competing interests.

Figures legends

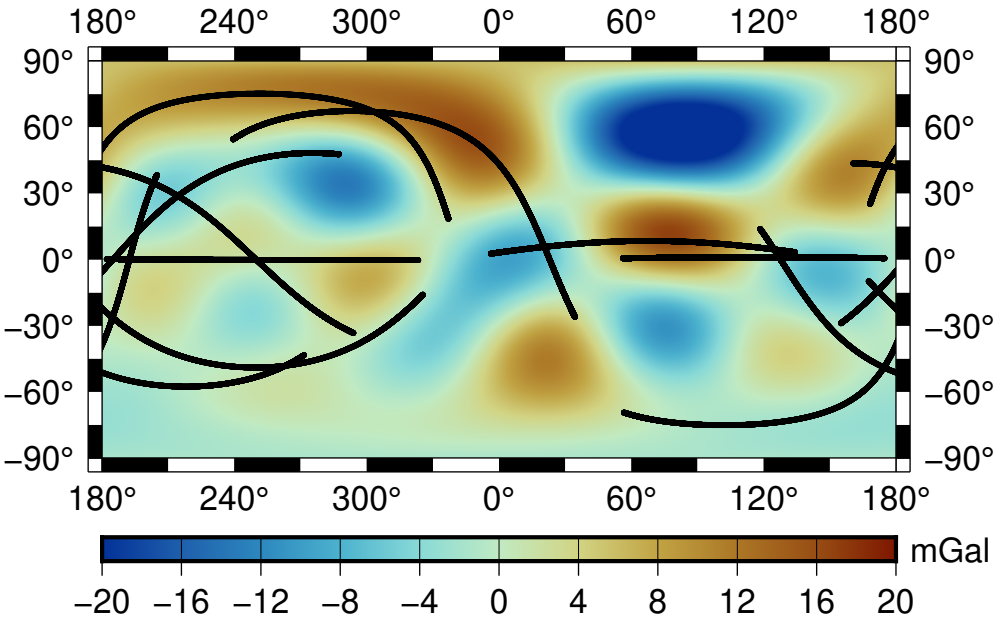

Fig. 1 Titan's gravity expressed as radial accelerations. The ground tracks of the flybys used in the determination of the gravity field model are indicated in black for altitudes less than 9,000 km. We set the coefficients $C_{2,0}$ and $C_{2,2}$ to zero for this map.

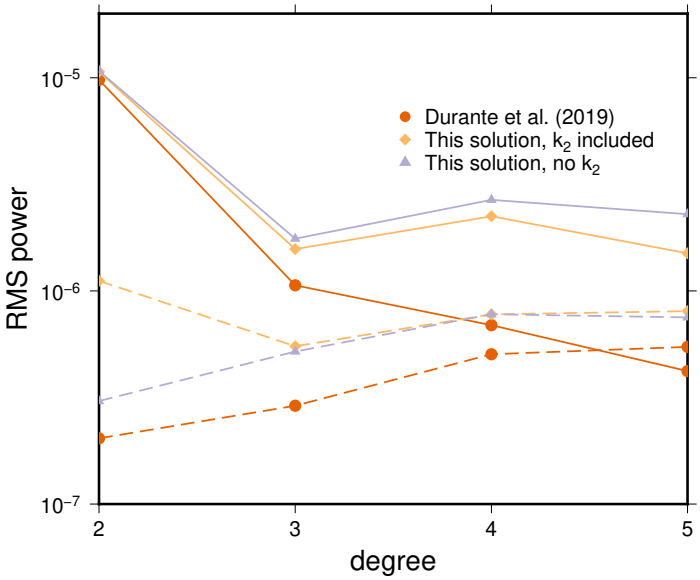

Fig. 2 Root-mean-square (RMS) power for Titan's gravity from our solution and the one from Durante et al. (2019) [3]. For this figure the coefficients were normalized following standard geodesy conventions [47]. The dashed lines indicate the RMS power for the formal errors.

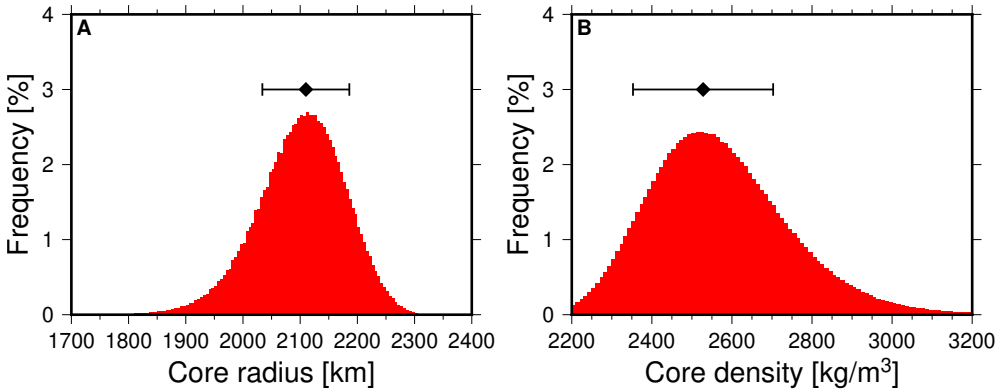

Fig. 3 Properties of Titan's core. A posteriori distributions (including the central value ± 1 standard deviation) of the core radius (A) and core density (B) for Titan as the results from our Markov Chain Monte Carlo analysis to match the moment of inertia, bulk density and Love number. We evaluated 500,000 models with 40 chains.

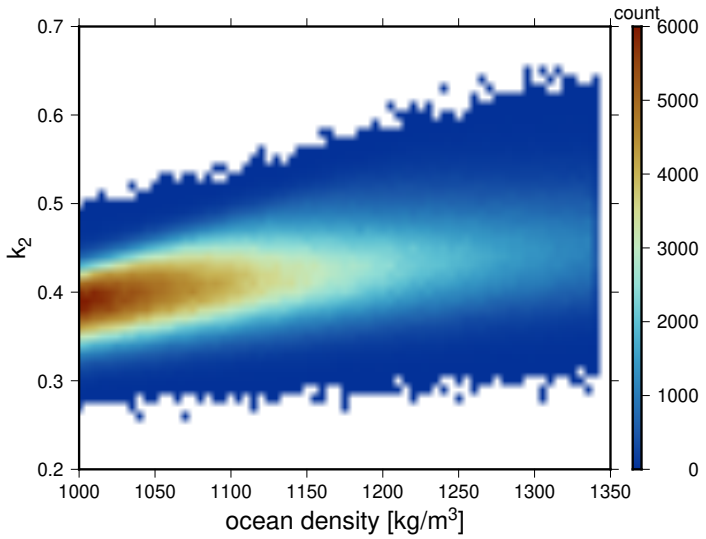

Fig. 4 Ocean density versus Love number k_2 for Titan. The results are displayed as a heat map using the counts from our Markov Chain Monte Carlo analysis.

References

[1] Iess, L. *et al.* Gravity Field, Shape, and Moment of Inertia of Titan. *Science* **327**, 1367–1369 (2010). Doi:10.1126/science.1182583.

[2] Tortora, P. *et al.* Rhea gravity field and interior modeling from Cassini data analysis. *Icarus* **264**, 264–273 (2016).

[3] Durante, D., Hemingway, D. J., Racioppa, P., Iess, L. & Stevenson, D. J. Titan's gravity field and interior structure after Cassini. *Icarus* **326**, 123–132 (2019).

[4] Zannoni, M., Hemingway, D., Gomez Casajus, L. & Tortora, P. The gravity field and interior structure of Dione. *Icarus* **345**, 113713 (2020).

[5] Iess, L. *et al.* Measurement and implications of Saturn's gravity field and ring mass. *Science* **364**, aat2965 (2019).

[6] Iess, L. *et al.* The Tides of Titan. *Science* **337**, 457–459 (2012). Doi:10.1126/science.1219631.

[7] Lunine, J. I. & Stevenson, D. J. Clathrate and ammonia hydrates at high pressure: Application to the origin of methane on Titan. *Icarus* **70**, 61–77 (1987).

[8] Grasset, O. & Sotin, C. The Cooling Rate of a Liquid Shell in Titan's Interior. *Icarus* **123**, 101–112 (1996).

[9] Grasset, O., Sotin, C. & Deschamps, F. On the internal structure and dynamics of Titan. *Planet. Sp. Sci.* **48**, 617–636 (2000).

[10] Sohl, F., Hussmann, H., Schwentker, B., Spohn, T. & Lorenz, R. D. Interior structure models and tidal Love numbers of Titan. *J. Geophys. Res.: Planets* **108**, 5130 (2003).

[11] Rappaport, N., Bertotti, B., Giampieri, G. & Anderson, J. D. Doppler Measurements of the Quadrupole Moments of Titan. *Icarus* **126**, 313–323 (1997).

[12] Rappaport, N. J. *et al.* Can Cassini detect a subsurface ocean in Titan from gravity measurements? *Icarus* **194**, 711–720 (2008).

[13] Sohl, F. *et al.* Structural and tidal models of Titan and inferences on cryovolcanism. *J. Geophys. Res.: Planets* **119**, 1013–1036 (2014).

[14] Sotin, C., Kalousová, K. & Tobie, G. Titan's Interior Structure and Dynamics After the Cassini-Huygens Mission. *Annu. Rev. Earth Planet. Sci.* **49** (2021).

[15] Stiles, B. W. *et al.* Determining Titan's Spin State from Cassini RADAR Images. *Astron. J.* **135**, 1669–1680 (2008). Doi:10.1088/0004-6256/135/5/1669.

[16] Zebker, H. A. *et al.* Size and Shape of Saturn's Moon Titan. *Science* **324**, 921 (2009).

[17] Mitri, G. *et al.* Shape, topography, gravity anomalies and tidal deformation of Titan. *Icarus* **236**, 169–177 (2014). Doi:10.1016/j.icarus.2014.03.018.

[18] Baland, R.-M., Tobie, G., Lefèvre, A. & Van Hoolst, T. Titan's internal structure inferred from its gravity field, shape, and rotation state. *Icarus* **237**, 29–41 (2014).

[19] Beuthe, M. Tidal Love numbers of membrane worlds: Europa, Titan, and Co. *Icarus* **258**, 239–266 (2015). Doi:10.1016/j.icarus.2015.06.008.

[20] Iess, L. *et al.* The Gravity Field and Interior Structure of Enceladus. *Science* **344**, 78–80 (2014). Doi:10.1126/science.1250551.

[21] Murray, C. & Dermott, S. *Solar System Dynamics* (Cambridge University Press, New York, USA, 1999).

[22] Meriggiola, R., Iess, L., Stiles, B. W., Lunine, J. I. & Mitri, G. The rotational dynamics of Titan from Cassini RADAR images. *Icarus* **275**, 183–192 (2016).

[23] Fortes, A. D. Titan's internal structure and the evolutionary consequences. *Planet. Sp. Sci.* **60**, 10–17 (2012). Doi:10.1016/j.pss.2011.04.010.

[24] Gao, P. & Stevenson, D. J. Nonhydrostatic effects and the determination of icy satellites' moment of inertia. *Icarus* **226**, 1185–1191 (2013). Doi:10.1016/j.icarus.2013.07.034.

[25] Coyette, A., Baland, R.-M. & Van Hoolst, T. Variations in rotation rate and polar motion of a non-hydrostatic Titan. *Icarus* **307**, 83–105 (2018).

[26] Zharkov, V. N., Leontjev, V. V. & Kozenko, V. A. Models, figures, and gravitational moments of the Galilean satellites of Jupiter and icy satellites of Saturn. *Icarus* **61**, 92–100 (1985).

[27] Asmar, S. W., Armstrong, J. W., Iess, L. & Tortora, P. Spacecraft Doppler tracking: Noise budget and accuracy achievable in precision radio science observations. *Radio Sci.* **40**, n/a–n/a (2005).

[28] Ermakov, A. I., Park, R. S. & Bills, B. G. Power Laws of Topography and Gravity Spectra of the Solar System Bodies. *J. Geophys. Res.: Planets* **123**, 2038–2064 (2018).

[29] Eanes, R., Schutz, B. & Tapley, B. Earth and ocean tide effects on Lageos and Starlette. *Proc. Ninth Int. Symp. Earth Tides* 239–249 (1983).

[30] McCarthy, D. D. & Petit, G. IERS Conventions (2003). *IERS Technical Note* **32** (2004).

[31] Vance, S. D. *et al.* Geophysical Investigations of Habitability in Ice-Covered Ocean Worlds. *J. Geophys. Res.: Planets* **123**, 180–205 (2018).

[32] Foreman-Mackey, D., Hogg, D. W., Lang, D. & Goodman, J. emcee: The MCMC Hammer. *Publ. Astron. Soc. Pac.* **125**, 306 (2013).

[33] Pavlis, D. E. & Nicholas, J. B. GEODYN II system description (vols. 1-5). contractor report, SGT Inc., Greenbelt, MD (2017). URL https://earth.gsfc.nasa.gov/geo/data/geodyn-documentation.

[34] Bertotti, B., Iess, L. & Tortora, P. A test of general relativity using radio links with the Cassini spacecraft. *Nature* **425**, 374–376 (2003).

[35] Archinal, B. A. *et al.* Report of the IAU Working Group on Cartographic Coordinates and Rotational Elements: 2015. *Celest. Mech. Dyn. Astron.* **130**, 22 (2018).

[36] Bellerose, J., Roth, D. & Criddle, K. The Cassini Mission: Reconstructing Thirteen Years of the Most Complex Gravity-Assist Trajectory Flown to Date. *2018 SpaceOps Conf.* (American Institute of Aeronautics and Astronautics, Marseille, France, 2018). URL https://arc.aiaa.org/doi/10.2514/6.2018-2646.

[37] Barbaglio, F., Armstrong, J. W. & Iess, L. Precise Doppler Measurements for Navigation and Planetary Geodesy Using Low Gain Antennas: Test Results from Cassini. *Proc. 23rd Int. Symp. Sp. Flight Dyn.* (Pasadena, California, USA, 2012). URL https://issfd.org/ISSFD_2012/ISSFD23_OD1_4.pdf.

[38] Montenbruck, O. & Gill, E. *Satellite Orbits* (Springer-Verlag, Berlin, 2000).

[39] Tapley, B., Schutz, B. & Born, G. *Statistical Orbit Determination* (Elsevier Academic Press, Burlington, MA., USA, 2004).

[40] Kusche, J. Noise variance estimation and optimal weight determination for GOCE gravity recovery. *Adv. Geosci.* **1**, 81–85 (2003). Doi:10.5194/adgeo-1-81-2003.

[41] Běhounková, M., Souček, O., Hron, J. & Čadek, O. Plume Activity and Tidal Deformation on Enceladus Influenced by Faults and Variable Ice Shell Thickness. *Astrobiology* **17**, 941–954 (2017).

[42] Hemingway, D. J. & Mittal, T. Enceladus's ice shell structure as a window on internal heat production. *Icarus* **332**, 111–131 (2019).

[43] Renaud, J. P. TidalPy (0.4.1) (2023). URL https://zenodo.org/record/7017560.

[44] Styczinski, M. J., Vance, S. D. & Melwani Daswani, M. Planetprofile: Self-consistent interior structure modeling for ocean worlds and rocky dwarf planets in python. *Earth Space Sci.* **10**, e2022EA002748 (2023). URL https://agupubs.onlinelibrary.wiley.com/doi/abs/10.1029/2022EA002748.

E2022EA002748 2022EA002748.

[45] Foreman-Mackey, D. corner.py: Scatterplot matrices in python. *J. Open Source Softw.* **1**, 24 (2016). URL https://doi.org/10.21105/joss.00024.

[46] Wessel, P., Smith, W. H. F., Scharroo, R., Luis, J. & Wobbe, F. Generic Mapping Tools: Improved Version Released. *EOS, Transactions American Geophysical Union* **94**, 409–410 (2013).

[47] Kaula, W. M. *Theory of Satellite Geodesy, applications of satellites to Geodesy* (Blaisdell Publishing Company, Waltham, MA., USA, 1966).